**Aalborg Universitet**

AALBORG UNIVERSITY
DENMARK

# Franz-Keldysh effect and electric field-induced second harmonic generation in graphene

*From one-dimensional nanoribbons to two-dimensional sheet*

Bonabi, Farzad; Pedersen, Thomas Garm

*Published in:*
Physical Review B

*DOI (link to publication from Publisher):*
10.1103/PhysRevB.99.045413

*Publication date:*
2019

*Document Version*
Publisher's PDF, also known as Version of record

Link to publication from Aalborg University

*Citation for published version (APA):*
Bonabi, F., & Pedersen, T. G. (2019). Franz-Keldysh effect and electric field-induced second harmonic generation in graphene: From one-dimensional nanoribbons to two-dimensional sheet. *Physical Review B*, *99*(4), [045413]. https://doi.org/10.1103/PhysRevB.99.045413

**General rights**
Copyright and moral rights for the publications made accessible in the public portal are retained by the authors and/or other copyright owners and it is a condition of accessing publications that users recognise and abide by the legal requirements associated with these rights.

- Users may download and print one copy of any publication from the public portal for the purpose of private study or research.
- You may not further distribute the material or use it for any profit-making activity or commercial gain
- You may freely distribute the URL identifying the publication in the public portal -

**Take down policy**
If you believe that this document breaches copyright please contact us at vbn@aub.aau.dk providing details, and we will remove access to the work immediately and investigate your claim.

# Franz-Keldysh effect and electric field-induced second harmonic generation in graphene: From one-dimensional nanoribbons to two-dimensional sheet

Farzad Bonabi and Thomas G. Pedersen
*Department of Materials and Production, Aalborg University, Skjernvej 4A, DK-9220 Aalborg East, Denmark*

(Received 23 August 2018; revised manuscript received 30 October 2018; published 9 January 2019)

It is well established that external electrostatic fields modify the electronic structure and optical response of materials. Modifications of the optical response of quasi-one-dimensional graphene nanoribbons (GNRs) depend strongly on the direction of the electrostatic field. While transverse fields primarily lift degeneracies in the band structure, longitudinal fields are responsible for considerable nonperturbative Franz-Keldysh effects. Also, electric fields break the inversion symmetry of GNRs and result in strong electric field-induced second harmonic generation. In this work, we study field-induced modifications of the linear and nonlinear optical response of narrow and wide semiconducting armchair GNRs (AGNRs). Both finite and infinite AGNRs with and without electrostatic fields are studied and length convergence is analyzed. Similarly, the width convergence of wide AGNRs to the two-dimensional graphene limit with and without longitudinal fields is investigated.

DOI: 10.1103/PhysRevB.99.045413

## I. INTRODUCTION

Graphene is an infinite two-dimensional sheet of carbon atoms with attractive features such as high electron mobility and tuneable conductivity [1]. Graphene nanoribbons (GNRs) are strips of graphene that can be synthesized as semiconductors with tunable band gaps [2] and, thus, are promising candidates for various electronic [3–7] and optical [8–10] applications. Such nanoribbons with various widths can be produced by unzipping carbon nanotubes as well as bottom-up synthesis and lithography [11–13]. The fabrication of semiconducting GNRs has been extended to atomically precise sub-10-nm widths [14], and further to ultranarrow sub-1-nm ribbons. [12,15,16]. Such ultranarrow GNRs have a sizable band gap and can potentially be employed in various electronic and optical applications. The electronic and optical properties of GNRs differ significantly from two- and three-dimensional carbon-based structures, due to their one-dimensional nature. In the presence of both electrostatic and optical fields, novel electro-optical effects enable applications such as phototransistors [17]. Weak static fields only have minor effects on the electronic states. In contrast, strong electrostatic fields in semiconductors result in nonperturbative Franz-Keldysh (FK) effects, including field-induced absorption below the band gap [18,19].

Several studies have investigated the optical response of GNRs with various edges, in particular, armchair GNRs (AGNRs) and zigzag GNRs (ZGNRs), with or without defects or chemical edge saturation [20–26]. Several publications have considered transversal electric fields in AGNRs and ZGNRs [27–32], multilayered GNRs [33–35] and boron nitride nanoribbons (BNNRs) [36]. Such static fields can reduce the band gap to a few meV in selected semiconducting AGNRs [27], while they open a gap in selected metallic ZGNRs [28]. Moreover, fields break the inversion symmetry and cause strong resonances in electroabsorption (EA) spectra in the low-energy limit [29], due to significant changes in the band structure of selected GNRs [31,32]. For multilayered GNRs, considerable changes in the band structure and edge states, as well as transformation from metallic to semiconducting behavior or vice versa, are seen [33–35]. Furthermore, similar results have been seen in BNNRs for a wider energy range than GNRs [36].

Although transversal electrostatic fields have important effects on the electronic structure and optical response of single- and multilayer GNRs and BNNRs, longitudinal static-field effects on these structures have not been considered yet. In carbon nanotubes with various chiralities, longitudinal electrostatic fields along the tube axis result in strong interband FK oscillations [37]. In Ref. [38], the authors have studied the effects of periodic longitudinal electric fields on AGNRs and ZGNRs optical responses and found modulations in the absorption spectra of these structures. The studied longitudinal fields are extended over up to eight GNR unit cells and produce a periodic modification of the Hamiltonian matrix. Thus, FK effects are not reflected in the obtained results due to the limited dc field periods in that paper. It is computationally rather costly to apply large dc field periods, as required to approach uniform fields, so this method is not an efficient way to calculate FK effects in periodic structures. Also, the second-order nonlinear optical response has not been considered yet because it is symmetrically forbidden in GNRs. Including electrostatic fields in these materials will break the inversion symmetry and result in electric field-induced second harmonic (EFISH) generation [39–41].

External electric fields also modify the optical response of two-dimensional graphene. External dc gates modify the Fermi energy and facilitate photocurrents in graphene, which are crucial for optical modulators and photodetectors, respectively [42]. Moreover, time-dependent electric fields open energy gaps in the quasienergy spectrum and are responsible for dynamical FK effects [43]. Applying strong electrostatic fields in graphene generates Wannier-Stark (WS) states within

 ©2019 American Physical Society

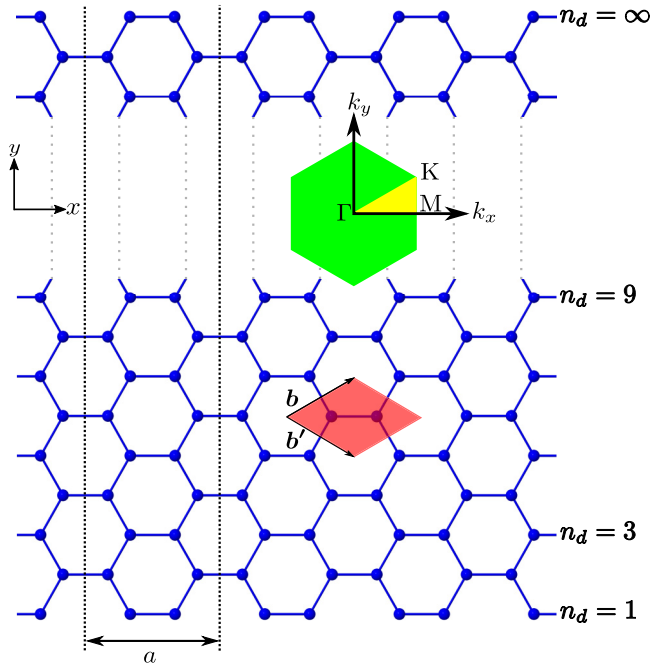


FIG. 1. Atomic structure of AGNRs with varying $n_d$ number of rows of carbon-carbon dimer bonds. Longitudinal and transversal axes are along the $x$ and $y$ directions, respectively. The black dashed lines show the AGNR unit cell with the length $a$ and the red diamond is the two-dimensional graphene unit cell with $\boldsymbol{b}$ and $\boldsymbol{b}'$ as unit vectors. The green hexagon and yellow triangle show full and irreducible Brillouin zone of graphene, respectively, and Γ, M, and K are high symmetry points in $k$ space.

valence and conduction bands and results in coupling between these states with anticrossing points, in which couplings are very strong near Dirac points [44]. Therefore, it is expected that the linear and nonlinear optical response of graphene show FK effects as a result of transitions between WS states. Furthermore, it is valuable to show that the optical response of quasi-one-dimensional GNRs with and without dc fields converges to two-dimensional graphene in the limit of sufficiently wide GNRs.

In the present work, we investigate the effects of strong electrostatic fields on the linear and nonlinear optical response of narrow and wide AGNRs and two-dimensional graphene. We restrict ourselves to AGNRs having atomically precise edges without defects or fluctuating widths. Figure 1 shows the schematic atomic structure of AGNRs with various widths as well as two-dimensional pristine graphene, using the AGNR-$n_d$ notation, in which $n_d$ is the number of carbon-carbon dimer bonds in the finite direction, i.e., $y$ direction for AGNRs and $n_d = \infty$ represents the two-dimensional graphene. We start from narrow AGNRs and take AGNR-3 and AGNR-9 and obtain their electronic structure and linear and nonlinear optical response with and without the presence of transversal $F^y_{\rm dc}$ and longitudinal $F^x_{\rm dc}$ dc fields. In our recent work, we computed FK effects for longitudinal electrostatic fields in simple two-band one-dimensional semiconductors [45]. To that end, we have followed methods in [46,47] and introduced a novel and computationally efficient density matrix method to calculate the optical response of infinite systems in $k$ space. Here, we generalize our method for studying FK effects and EFISH in any multiband semiconductor. Then, we apply this method to narrow but infinitely long AGNRs and compare the obtained results with those of finite-length AGNRs. Next, we increase the width from medium to wide AGNR by taking AGNR-45, AGNR-90, AGNR-180, and AGNR-390 and compare their linear and nonlinear optical response with those of two-dimensional graphene. This comparison is important because it shows that our method is applicable from ultranarrow one-dimensional semiconductors to ultrawide ones, where features of two-dimensional systems are expected. To enable such comparison, we show how the response of one-dimensional semiconductors under longitudinal dc fields is extended to two-dimensional systems. This is done by dividing $k$ space into two directions for two-dimensional systems, i.e., parallel and perpendicular to the dc field direction and utilizing periodicity in the perpendicular direction.

The remainder of this paper is organized as follows: in Sec. II, we calculate the electronic structure of AGNRs using the tight-binding method. Then, we present the linear and nonlinear optical response for finite and infinite multiband semiconductors and two-dimensional graphene with and without static electric fields. Subsequently, results of calculations are presented in Sec. III. Finally, Sec. IV summarizes methods and obtained results in this paper.

## II. THEORY AND METHODS

### A. Electronic structure

We obtain the electronic structure of both finite and infinite AGNRs and two-dimensional graphene using the orthogonal nearest neighbor tight-binding model with one $\pi$ orbital per carbon atom and $\pi$-$\pi$ hopping energy set at $\gamma_0 = -2.97$ eV [48]. The lattice constant is $|\boldsymbol{b}| \equiv b = 2.46$ Å for graphene and $a = 4.26$ Å for the AGNRs. The number of unit cells $N$ is varied between 50 and 400 for finite AGNRs in order to study the convergence toward infinite nanoribbons. Dangling bonds at the GNR edges are assumed to be saturated with hydrogen atoms. The presence of carbon-hydrogen bonds leads to shortened carbon-carbon bonds at the edges, resulting in slightly increased $\pi$-$\pi$ hopping energy for these bonds [20]. We ignore such complications because they only produce minor modifications of the electronic structure and do not affect any qualitative results in this work.

For infinite AGNRs and two-dimensional graphene as shown in Fig. 1, the Hamiltonian matrix is constructed from Bloch sums considering one- and two-dimensional $k$ space, respectively. We only consider the effect of transversal electrostatic fields in narrow AGNRs, i.e., AGNR-3 and AGNR-9 and calculate their electronic structure by adding the dc field Hamiltonian $eyF^y_{\rm dc}$ to their unperturbed Hamiltonian. Here, $-e$ is the electron charge and $y$ is the position of atoms along the $y$ axis. Band structures of these narrow AGNRs with and without transversal dc fields are plotted in Fig. 2. In the nearest neighbor tight-binding model, band gap energies are approximately 2.46 eV and 1.04 eV for AGNR-3 and AGNR-9, respectively. The dc field introduces on-site energies in the Hamiltonian, and results in coupling between bands, however,

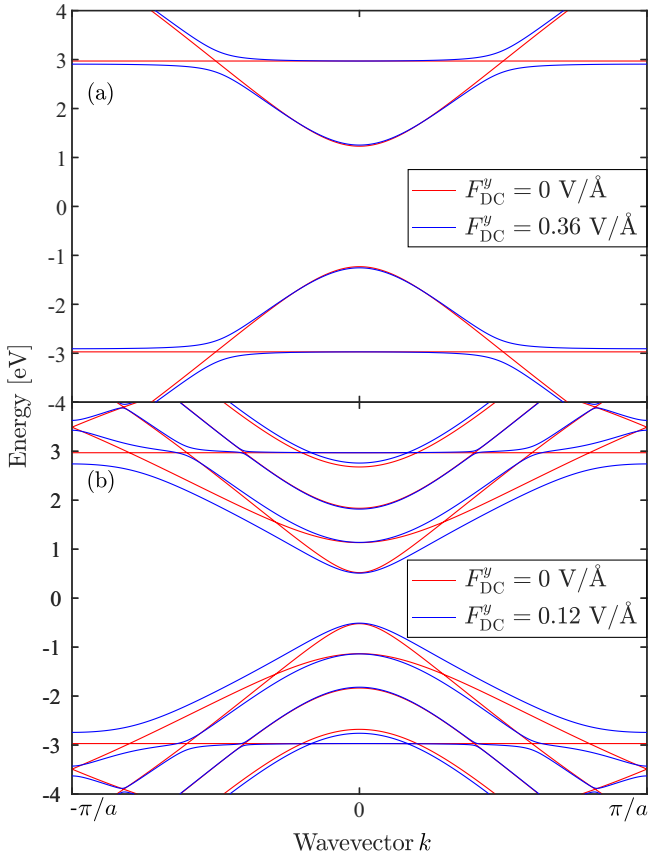


FIG. 2. Band structure of (a) AGNR-3 and (b) AGNR-9 in the nearest neighbor tight-binding model. The red curves show the band structures under $F^y_{\rm dc} = 0$ and the blue curves under $F^y_{\rm dc} = 0.36\,{\rm V/Å}$ for AGNR-3 and $F^y_{\rm dc} = 0.12\,{\rm V/Å}$ for AGNR-9.

the field should be rather strong to make considerable changes to the band structure. Thus, due to additional transitions caused by the dc field, new features in the optical response are expected. We use $F^y_{\rm dc} = 0.36\,{\rm V/Å}$ for AGNR-3 and $F^y_{\rm dc} = 0.12\,{\rm V/Å}$ for AGNR-9. The higher field strength for AGNR-3 is because this system requires larger dc field strength to show considerable changes in the band structure. The reason is that the total induced dipole moment from external dc fields gets stronger with increasing AGNR width due to the increase in the number of atoms, so the effects of transversal dc fields are more pronounced in wider AGNRs for a fixed dc field strength.

### B. Optical response

Here, we calculate the linear and nonlinear optical response of finite and infinite systems for optical fields oriented along their longitudinal direction. These responses can be investigated by adding an optical field Hamiltonian $\hat{H}_t = e\hat{x}F_t$ to the unperturbed Hamiltonian $\hat{H}_0$,

$$\hat{H} = \hat{H}_0 + \hat{H}_t. \tag{1}$$

Here, the dipole moment along the $x$ axis $e\hat{x}$ can be calculated using the position operator $\hat{x}$ for a finite system and subsequently applied in the optical conductivity equation [45],

$$\sigma_1^{\rm finite}(\omega) = -2ie^2\omega \sum_{m,n} f(E_n)|x_{nm}|^2 \frac{E_{mn}}{E_{mn}^2 - \hbar^2\omega^2}, \tag{2}$$

where $\hbar\omega$ is the photon energy, $E_{mn}$ is the energy difference of states $m$ and $n$, and $f(E_n)$ is the Fermi-Dirac distribution function. Throughout this study, we add a phenomenological damping term $i\hbar\Gamma$ to the photon energy and take $\hbar\Gamma = 50$ meV and consider cold and clean (intrinsic) AGNRs.

In the case of infinite AGNRs, the interband part of Eq. (2) is rewritten in $k$ space using well-defined momentum matrix elements instead of dipole moment matrix elements via $x_{nmk} = \hbar p_{nmk}/imE_{nmk}$ [49]. This expression can be obtained from the commutator relation between the interband part of the position operator and Hamiltonian via $[\hat{H}_0, \hat{x}] = \hbar\hat{p}/im$. We take the Fermi level in the middle of the gap and consider cold and clean systems. consequently, in the absence of longitudinal dc fields, there are no intraband contributions to the linear optical response. Thus, the interband linear conductivity is

$$\sigma_1^{\infty}(\omega) = \frac{-2ie^2\hbar^2\omega}{m^2} \sum_{m\neq n,k} f(E_{nk}) \frac{|p_{nmk}|^2}{E_{mnk}\left(E_{mnk}^2 - \hbar^2\omega^2\right)}. \tag{3}$$

Summation over $k$ should be understood as the discretization of an integral in $k$ space over $N_k$ points with spacing $\Delta k = 2\pi/N_k a$. We choose $N_k$ varying between 1000 and 5000 to get converged results for infinite AGNRs and graphene. In the case of two-dimensional graphene, $k$ is replaced by the vector $\boldsymbol{k}$ having both $x$ and $y$ components.

Upon additional iteration using the perturbation formalism, the second-order nonlinear optical conductivity is

$$\sigma_2^{\rm finite}(\omega) = -6ie^3\omega \sum_{m,n,l} f(E_n) x_{nm}x_{ml}x_{ln} \times \frac{\hbar\omega E_{ml} + E_{mn}E_{ln}}{(E_{mn} - 2\hbar\omega)(E_{ln} + 2\hbar\omega)(E_{ln} - \hbar\omega)(E_{mn} + \hbar\omega)}. \tag{4}$$

Throughout this paper, we only consider the diagonal $\sigma_1 = \sigma_{xx}$ and $\sigma_2 = \sigma_{xxx}$ components of the linear and nonlinear optical conductivity tensor.

### C. Electrostatic field and Franz-Keldysh effects

In this section, we investigate effects of strong static electric fields $\boldsymbol{F}_{\rm dc}$ on the linear and nonlinear optical response of one- and two-dimensional semiconductors. In particular, for longitudinal fields, our focus is on the nonperturbative effects of strong fields. However, in the case of extremely strong fields, significant charge is transferred between the ends of the structure. For a finite system of length $L$, this occurs if the potential difference between the ends $eLF_{\rm dc}$ exceeds the band gap $E_g$. In this case, the tilted potential due to the dc field will lead to a Fermi level crossing both valence and conduction bands. In the present work, to avoid the complications of charge transfer, we mainly restrict the analysis to

structures, for which $eLF_{\rm dc} < E_g$. For illustrational purposes, however, longer structures are briefly considered in order to highlight the differences between the two scenarios. Also, importantly, we wish to explore the $k$-space formalism as a computationally efficient alternative to modeling of finite but long structures. The $k$-space formalism essentially assumes infinitely long structures ($L \to \infty$), for which the condition $eLF_{\rm dc} < E_g$ is clearly not satisfied. We wish to investigate, however, whether this approach is an acceptable approximation for finite systems satisfying $eLF_{\rm dc} < E_g$. As will be shown below, this is indeed the case provided intraband transitions are omitted in the $k$-space approach. Thus, we use two different approaches for finite and infinite systems, respectively. For finite structures, the effect of electrostatic fields can be calculated by adding an electrostatic Hamiltonian to the unperturbed Hamiltonian,

$$\hat{H} = \hat{H}_0 + e\boldsymbol{F}_{\rm dc} \cdot \hat{\boldsymbol{r}}. \tag{5}$$

Eigenvalues and eigenvectors of this Hamiltonian are used to calculate transition energies and dipole moment matrix elements. Substituting these results into Eq. (2) and Eq. (4), the finite linear and nonlinear optical conductivities are computed, respectively.

For one-dimensional infinite semiconductors like AGNRs, if the electrostatic field is transversal $\boldsymbol{F}_{\rm dc} = F^y_{\rm dc}\boldsymbol{e}_y$, i.e., along the finite direction of systems, Eq. (5) is used to obtain eigenvalues and eigenvectors for calculating transition energies and momentum matrix elements. Applying these results in Eq. (3), the linear optical conductivity is calculated.

For the longitudinal electrostatic field $\boldsymbol{F}_{\rm dc} = F^x_{\rm dc}\boldsymbol{e}_x$, i.e., along the infinite direction of the system, we follow the density matrix $\rho$ formalism for a general multiband semiconductor to study the nonperturbative field effects on the linear and nonlinear optical response. This approach is an expansion of the method in our previous study for a two-band semiconductor [45]. The procedure is similar to Ref. [45], though the expressions get more complicated for the multiband model. There are no degenerate bands in AGNRs, hence, the field-induced coupling between bands can be ignored [50]. As an approximation, we take a pair of band $(n, m)$ and write the WS expression for this pair and then sum the contribution of all band pairs to solve the problem. The WS equation is $H^{\rm WS}_{mn}\psi^{(p)}_{mnk} = E^{(p)}_{mn}\psi^{(p)}_{mnk}$, where

$$H^{\rm WS}_{mn} = E_{mnk} + ieF^x_{\rm dc}\left(\frac{d}{dk} - i(\Omega_{mmk} - \Omega_{nnk})\right). \tag{6}$$

Here, $p$ is the index of a WS band pair, $E_{mnk} = E_{mk} - E_{nk}$ is the transition energy, and $\Omega_{mmk} - \Omega_{nnk}$ is the Berry connection [47] between the bands. The eigenstate for the selected band pair can be expressed by

$$\psi^{(p)}_{mnk} = \frac{1}{\sqrt{K_0}}\exp\left\{-\frac{i}{eF^x_{\rm dc}}\left(E^{(p)}_{mn}k - \int_0^k E_{mnk'}dk'\right)\right\}, \tag{7}$$

where $K_0$ is the width of the first Brillouin zone along the direction of the dc field, which is $K_0 = 2\pi/a$ for AGNRs and $K_0 = 4\pi/\sqrt{3}b$ for graphene. We follow the procedure in Ref. [45] to derive energy differences between WS states $E^{(p)}_{mn} = 2\pi peF^x_{\rm dc}/K_0 + 1/K_0\int_0^{K_0} E_{mnk}dk$ and write the equation of motion for diagonal density matrix elements $f_{nk} \equiv \rho_{nnk}$, which correspond to the population, and off-diagonal elements $\rho_{mnk}$, which describe the coherence,

$$\begin{aligned} &-i\hbar\frac{d\rho_{mnk}}{dt} + E_{mnk}\rho_{mnk} \\ &\quad = -ie\left(F^x_{\rm dc} + F_t\right)(\rho_{mnk})_{;k} + e\left(F^x_{\rm dc} + F_t\right) \\ &\qquad \times \sum_l \{\rho_{mlk}\Omega_{lnk}\bar{\delta}_{ln} - \Omega_{mlk}\rho_{lnk}\bar{\delta}_{ml}\}, \end{aligned} \tag{8}$$

where $\delta_{mn}$ is the Kronecker delta, $\bar{\delta}_{mn} = 1 - \delta_{mn}$ is 0 for $m = n$ and 1 for $m \neq n$, and $(\rho_{mnk})_{;k}$ is the generalized derivative of $\rho_{mnk}$ which can be written as $(\rho_{mnk})_{;k} = d\rho_{mnk}/dk - i(\Omega_{mmk} - \Omega_{nnk})\rho_{mnk}$.

We keep the assumption of a cold and clean semiconductor, i.e., $df_{nk}/dk \approx 0$, and also ignore terms $F^x_{\rm dc}\Omega_{mn}$ which are related to the direct interband coupling caused by the static field. Then, Eq. (8) is rewritten as

$$\begin{aligned} &-i\hbar\frac{d\rho_{mnk}}{dt} + H_{\rm WS}[\rho_{mnk}] \\ &\quad = -ieF_t(\rho_{mnk})_{;k} + eF_t\sum_l\{\rho_{mlk}\Omega_{lnk}\bar{\delta}_{ln} - \Omega_{mlk}\rho_{lnk}\bar{\delta}_{ml}\}. \end{aligned} \tag{9}$$

This equation is solved by the Green's function equation and its Fourier transformation and using the harmonic behavior of density matrix and optical fields as introduced in Ref. [45] for different orders of the density matrix. These result in $f^{(\omega)}_{nk} = 0$ and

$$\rho^{(\omega)}_{mnk} = -eF_\omega\bar{\delta}_{mn}\int G^{(\omega)}_{mn}(k,k')\Omega_{mnk'}f^{(0)}_{nmk'}dk'. \tag{10}$$

Here, $f^{(0)}_{nmk} = f^{(0)}_{nk} - f^{(0)}_{mk}$ is the population difference between the two bands. With a second iteration,

$$\begin{aligned} \rho^{(2\omega)}_{mnk} = &-e^2F^2_\omega\int G^{(2\omega)}_{mn}(k,k') \\ &\times\left[i\int\left\{G^{(\omega)}_{mn}(k',k'')\Omega_{mnk''}f^{(0)}_{nmk''}\bar{\delta}_{mn}dk''\right\}_{;k'}\right. \\ &+\sum_l\left\{\Omega_{lnk'}\bar{\delta}_{ln}\int G^{(\omega)}_{ln}(k',k'')\Omega_{mlk''}f^{(0)}_{lmk''}\bar{\delta}_{ml}dk''\right. \\ &\left.\left.-\Omega_{mlk'}\bar{\delta}_{ml}\int G^{(\omega)}_{ml}(k',k'')\Omega_{lnk''}f^{(0)}_{nlk''}\bar{\delta}_{ln}dk''\right\}\right]dk'. \end{aligned} \tag{11}$$

$$\begin{aligned} f^{(2\omega)}_{nk} = -\frac{e^2F^2_\omega}{\hbar\omega}\sum_l&\left\{\Omega_{lnk}\int G^{(\omega)}_{nl}(k,k')\Omega_{nlk'}f^{(0)}_{lnk'}\bar{\delta}_{nl}dk'\right. \\ &\left.-\Omega_{nlk}\int G^{(\omega)}_{ln}(k,k')\Omega_{lnk'}f^{(0)}_{nlk'}\bar{\delta}_{ln}dk'\right\}. \end{aligned} \tag{12}$$

The induced current up to the second order is calculated using these density matrix equations. To simplify the expressions, inter- and intraband terms are separated

according to

$$j_t = -\frac{e}{\pi m}\int \sum_{mn} p_{nmk}\rho_{mnk}dk$$
$$= -\frac{e}{\pi m}\int \left\{\sum_{m\neq n} p_{nmk}\rho_{mnk} + \sum_{n} p_{nnk}\rho_{nnk}\right\}dk. \quad (13)$$

We Fourier transform the current introduced in Ref. [45] and divide band indices $(m, n, l)$ into valence and conduction band indices $(v, c)$ and apply the cold and clean semiconductor condition to the Fermi-Dirac function $f^{(0)}_{mnk}$. After these manipulations,

$$\sigma_1(\omega) = \frac{e^2}{\pi m}\sum_{c,v}\sum_{p}\frac{P^{(p)}_{vc}O^{(p)}_{cv}}{E^{(p)}_{cv}-\hbar\omega} + (\omega\rightarrow -\omega)^*. \quad (14)$$

$$\sigma_2^{(eeie)}(\omega) = \frac{ie^3}{\pi m}\sum_{c,v}\sum_{p,q}\frac{P^{(p)}_{vc}O^{(q)}_{cv}Q^{(pq)}_{cv}}{\left(E^{(p)}_{cv}-2\hbar\omega\right)\left(E^{(q)}_{cv}-\hbar\omega\right)} + (\omega\rightarrow -\omega)^*. \quad (15)$$

$$\sigma_2^{(ieee)}(\omega) = \frac{e^3}{2\pi m\hbar\omega}\sum_{c,v}\sum_{p}\frac{R^{(p)}_{vc}O^{(p)}_{cv}}{E^{(p)}_{cv}-\hbar\omega} + (\omega\rightarrow -\omega)^*. \quad (16)$$

$$\sigma_2^{(iiee)}(\omega) = \frac{e^3}{\pi m}\sum_{c\neq c',v\neq v'}\sum_{p,q}\left\{\frac{P^{(p)}_{v'c}O^{(q)}_{cv}M^{(pq)}_{vv'}}{\left(E^{(p)}_{cv'}-2\hbar\omega\right)\left(E^{(q)}_{cv}-\hbar\omega\right)} - \frac{P^{(p)}_{vc'}O^{(q)}_{cv}M^{(pq)}_{c'c}}{\left(E^{(p)}_{c'v}-2\hbar\omega\right)\left(E^{(q)}_{cv}-\hbar\omega\right)} + \frac{P^{(p)}_{c'c}O^{(q)}_{cv}M^{(pq)}_{vc'}}{\left(E^{(p)}_{cc'}-2\hbar\omega\right)\left(E^{(q)}_{cv}-\hbar\omega\right)} - \frac{P^{(p)}_{vv'}O^{(q)}_{cv}M^{(pq)}_{v'c}}{\left(E^{(p)}_{v'v}-2\hbar\omega\right)\left(E^{(q)}_{cv}-\hbar\omega\right)}\right\} + (\omega\rightarrow -\omega)^*. \quad (17)$$

These expressions are written in WS notation as

$$P^{(p)}_{mn} = \int \psi^{(p)}_{mnk}p_{mnk}dk,\ O^{(p)}_{mn} = \int \psi^{(p)*}_{mnk}\Omega_{mnk}dk,$$
$$Q^{(pq)}_{mn} = \int \psi^{(q)*}_{mnk}(\psi^{(p)}_{mnk})_{;k}dk,$$
$$M^{(pq)}_{mn} = \int \psi^{(q)*}_{mnk}\left(\psi^{(p)}_{mnk}\right)\Omega_{mnk}dk,$$
$$R^{(p)}_{mn} = \int \psi^{(p)}_{mnk}(p_{mmk}-p_{nnk})\Omega_{mnk}dk. \quad (18)$$

Here, Eq. (14) is the linear optical conductivity and Eqs. (15)–(17) are different contributions of mixed inter- and intraband second-order nonlinear optical conductivity. These equations can be reduced to Eqs. (31) and (32) in Ref. [45], if a two-band system is considered. In the two-band model, Eq. (17) is absent. This contribution is also zero for our AGNRs since, for a cold and clean semiconductor, all $(v, v')$ and $(c, c')$ contributions are zero for $v\neq v'$ and $c\neq c'$. We use $O^{(p)}_{mn} = \hbar P^{(p)}_{mn}/(imE^{(p)}_{mn})$ and write Eq. (14) as

$$\sigma_1(\omega) = \frac{-i\hbar^2eK_0\omega}{\pi F^x_{\rm dc}m^2}\sum_{c,v}\sum_{p}\frac{\left|P^{(p)}_{vc}\right|^2}{E^{(p)2}_{cv}-\hbar^2\omega^2}. \quad (19)$$

The above expressions are written for one-dimensional systems, in which $k$ and $F_{dc}$ are along the periodic direction. In the case of two-dimensional graphene, $\boldsymbol{k}$ is a vector. Because the dc field is along the $x$ direction, $\boldsymbol{k}$ can be divided into two components $k_x$ and $k_y$ along and perpendicular to the field, respectively. For each $k_y$ point, the obtained expressions for the linear and nonlinear optical conductivity are valid. Thus, the two-dimensional linear optical conductivity follows from a summation of Eq. (19) over all $k_y$ points,

$$\sigma_1(\omega) = \frac{-i\hbar^2eK_0\omega}{\pi F^x_{\rm dc}m^2}\sum_{k_y}\sum_{c,v}\sum_{p}\frac{\left|P^{(p)}_{vck_y}\right|^2}{E^{(p)2}_{cvk_y}-\hbar^2\omega^2}. \quad (20)$$

$P^{(p)}_{vck_y}$ and $E^{(p)}_{cvk_y}$ are obtained from Eq. (18) and the WS energy difference $E^{(p)}_{mn}$, respectively, for each $k_y$ point. Similar modifications are applied to the nonlinear response functions.

## III. RESULTS AND DISCUSSION

### A. Finite and infinite narrow AGNRs

As a starting point, we calculate the linear optical response for both finite and infinite AGNRs without external dc fields. To this end, energies and dipole matrix elements are calculated for finite AGNRs with 50, 150, and 400 unit cells, and energy band structure and momentum matrix elements for infinite AGNRs. Applying these results in Eqs. (2) and (3), the real part of the linear optical conductivity per length $L = Na$, corresponding to the absorption, is shown in Fig. 3 taking the unit cell number for infinite systems as $N = N_k$. The first resonance for each AGNR corresponds to the transition at an energy equal to the band gap of the system. The additional peaks in AGNR-9 are the result of allowed transitions between valence and conduction bands with energies larger than the band gap. Also, optical transitions between the flat valence and conduction bands in Fig. 2 are responsible for the symmetric peak at 5.94 eV. With the increase of the number of unit cells, the finite system response converges to that of the infinite structure. The observed oscillations for the 50-unit cell structure are due to finite-size effects larger than the chosen broadening. [45].

To investigate the effects of electrostatic fields, we first apply the field in the transversal direction $F^y_{\rm dc} = 0.36$ V/Å for AGNR-3 and $F^y_{\rm dc} = 0.12$ V/Å for AGNR-9. We then calculate the linear optical conductivity for finite and infinite systems as shown in Fig. 4. The figure shows that for both AGNRs, the response of finite structures converges to that of infinite ones as the number of unit cells is increased. The linear optical conductivity with and without dc fields is plotted in Fig. 5 to illustrate the effects of the transversal dc fields on the optical response. The changes in the optical response can be explained by modifications in the AGNR band structure as illustrated in Fig. 2, especially near band crossings, where the field lifts the

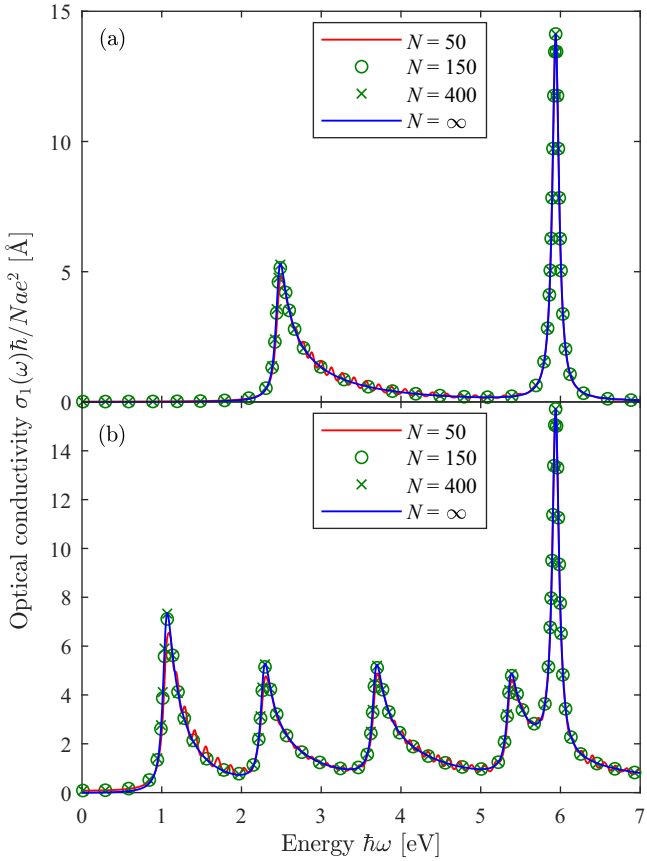


FIG. 3. Real part of linear optical conductivity of finite and infinite (a) AGNR-3 and (b) AGNR-9.

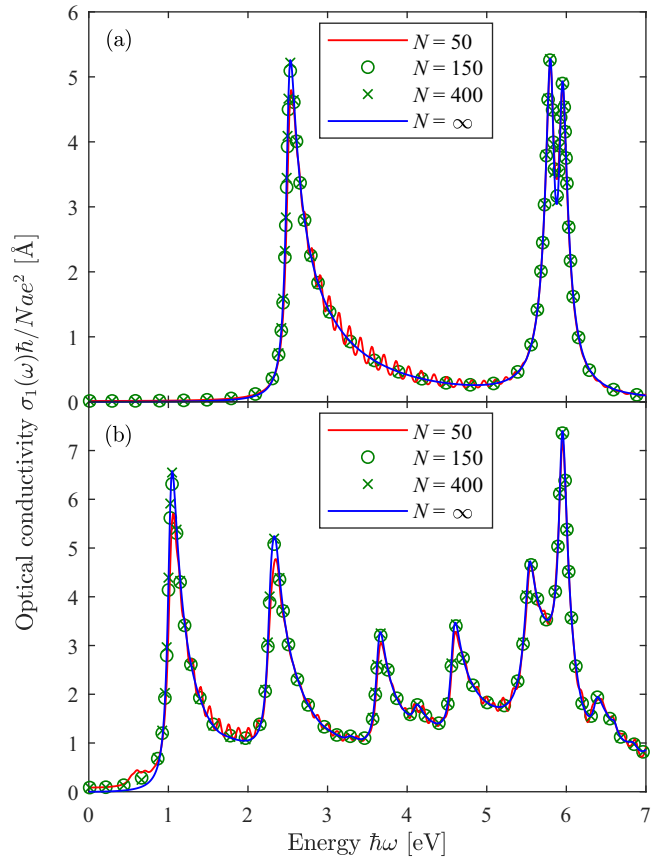


FIG. 4. Real part of linear optical conductivity of finite and infinite (a) AGNR-3 and (b) AGNR-9 under a transversal electrostatic field $F^y_{\rm dc} = 0.36$ V/Å for AGNR-3 and $F^y_{\rm dc} = 0.12$ V/Å for AGNR-9.

degeneracy. These changes introduce new transitions which appear as new peaks and modify both amplitude and position of the peaks in Fig. 5. These results agree qualitatively with the results for AGNR-7 in Ref. [38] and AGNR-156 in Ref. [31].

Next, we apply a longitudinal electrostatic field $F^x_{\rm dc} = 0.01\,{\rm V/Å}$ to narrow AGNRs. For this field direction, we consider a field strength much less than the one used for the transversal fields geometry. This is because, for a fixed dc field strength, the total induced dipole moment in the infinite direction is much stronger than the finite direction. As expected, the longitudinal field causes FK effects in the linear optical response. Again, we use Eq. (2) based on the Hamiltonian in Eq. (5), and Eq. (19) in order to calculate the linear optical conductivity for finite structures with 50, 150, and 400 unit cells and infinite AGNR-3 and AGNR-9 in Fig. 6. Comparing this figure to Fig. 4 for both AGNRs, FK oscillations for photon energies larger than the band gap energy are seen. Oscillations continue to appear after each major peak in the figure. The reason is that every pair of valence and conduction bands splits into WS states, and transitions occur between these states. In an effective mass model, these oscillations can be explained by the Airy function behavior of the optical response under the effect of dc fields [51]. Moreover, each AGNR has an exponential tail in the optical response below the band gap energy, which is due to the field-induced absorption in this energy region [51]. It may also be noted that the peaks are slightly blue-shifted due to changes in the transition energies between allowed valence and conduction states under the field.

The spectra in Fig. 6 show a considerable optical response in the low-energy range $\hbar\omega < 0.5\,{\rm eV}$ for long finite AGNRs ($N = 150$ and $N = 400$), while no such low-energy response is found for $N = 50$ and infinite structures. The origin of this difference lies in the fact that the condition $eLF^x_{\rm dc} < E_g$ is only satisfied for $N = 50$ AGNR-3 structure with $F^x_{\rm dc} = 0.01\,{\rm V/Å}$. In all other cases considered in Fig. 6, the Fermi level crosses several valence and conduction bands, leading to a considerable intraband optical response, however, this response is very weak for $N = 50$ AGNR-9 because the Fermi level crosses few states of this structure. For infinite systems, the intraband response can be captured by adding transitions within $(v, v)$ and $(c, c)$ band pairs to Eq. (19), resulting in a similar strong intraband response at low photon energy. We stress, however, that such large intraband response is an artifact of ignoring charge transfer. Hence, as shown in Fig. 6, the physically correct behavior in the $k$-space approach is found by omitting intraband terms.

Due to the computational efficiency of the $k$-space approach, it is important to investigate whether it is an accurate model of finite (but long) systems restricted by $eLF^x_{\rm dc} < E_g$, so that no charge transfer occurs under longitudinal dc fields.

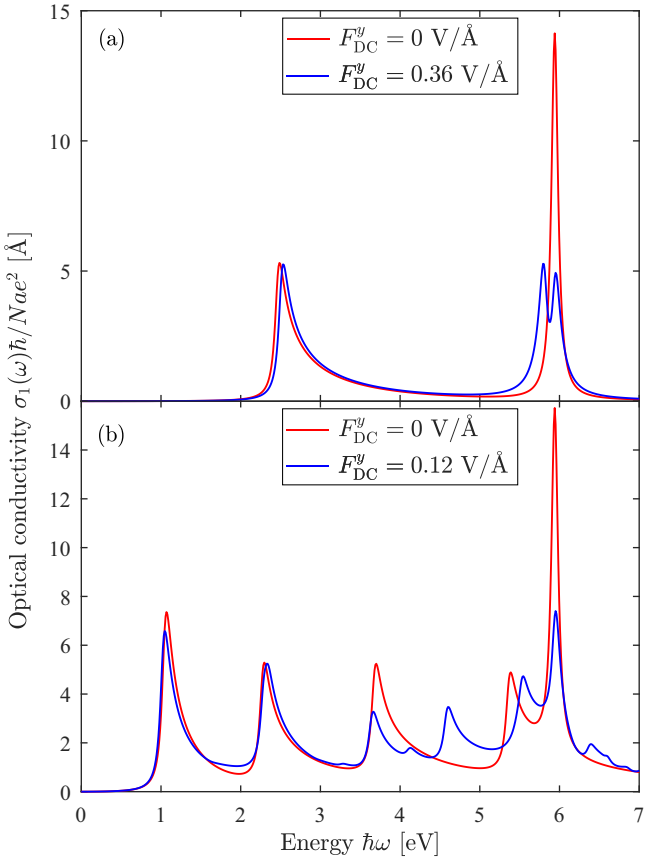


FIG. 5. Real part of linear optical conductivity of infinite (a) AGNR-3 and (b) AGNR-9 with and without transversal electrostatic field $F^y_{\rm dc} = 0.36$ V/Å for AGNR-3 and $F^y_{\rm dc} = 0.12$ V/Å for AGNR-9.

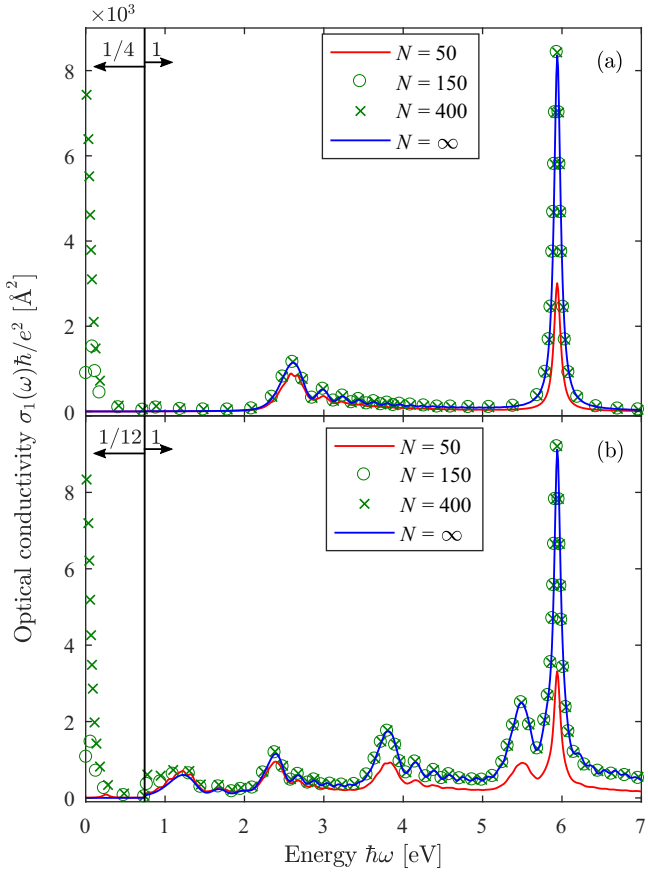


FIG. 6. Real part of linear optical conductivity for finite and infinite (a) AGNR-3 and (b) AGNR-9 under the effect of a longitudinal electrostatic field $F^x_{\rm dc} = 0.01$ V/Å. Note that the low-energy parts of the spectra have been down-scaled.

As seen in Fig. 6, the response of the $N = 50$ structures is in reasonable agreement with that of infinite systems. The location of all resonances is correctly reproduced for both AGNR-3 and AGNR-9. However, for AGNR-9, the $k$-space approach significantly overestimates the magnitude of the conductivity. Clearly, a smaller electric field allows for longer finite structures before charge transfer is observed. Thus, better agreement between finite and infinite cases is expected if a weaker field combined with longer structures is considered. To this end, Fig. 7 shows the linear optical conductivity for finite and infinite AGNR-3 under $F^x_{\rm dc} = 0.003$ V/Å. Reducing the field strength enables us to increase the finite system length up to $N = 200$ unit cells without violating the $eLF^x_{\rm dc} < E_g$ condition. Moreover, in Fig. 7, all unphysical intraband $(v, v)$ and $(c, c)$ contributions are excluded. As a result, for AGNR-3 the $N = 200$ spectrum is in good agreement with that of the infinite structure, especially near the band gap. This demonstrates the applicability of the $k$-space approach for cases of practical relevance.

Finally, we calculate the second-order nonlinear optical conductivity for finite and infinite narrow AGNRs. Transversal electrostatic fields do not break the inversion symmetry along the $x$ direction of our selected AGNRs, which are of type AGNR-3$n_d$, so their second-order nonlinear response is zero. However, this symmetry is broken for AGNR-3$n_d + 1$ and AGNR-3$n_d + 2$ types. In addition, $x$-inversion symmetry is broken for AGNR-3$n_d$ structures under longitudinal dc fields. Applying the dc Hamiltonian in Eq. (5), a longitudinal electrostatic field $F^x_{\rm dc} = 0.01$ V/Å is applied to calculate the second-order nonlinear optical conductivity for finite AGNRs from Eq. (4). Then, Eqs. (16) and (17) are used to compute the second-order nonlinear optical conductivity for different mixed inter- and intraband contributions for infinite AGNRs. Also, intraband contributions within $(v, v)$ and $(c, c)$ band pairs are omitted for infinite structures, leading to vanishing response in the low-energy limit. Figure 8 shows the real part of the second-order nonlinear optical conductivity for AGNR-3 and AGNR-9. In both AGNRs, EFISH spectra show several similarities to the FK effect in the linear response. Thus, oscillatory modulations above the $\omega$ and $2\omega$ resonances with different periods are observed. These results agree with Ref. [52], where exponential decay below and oscillatory behavior above each one- and two-photon absorptions are expected. In the case of AGNR-9, which has more allowed transitions between valence and conduction bands, the period and strengths of oscillations are the results of the mixture of different one- and two-photon absorptions between energy states belong to each valence and conduction band pair, so oscillatory features are not as prominent as in AGNR-3. Similar to the linear response, in both systems, there is a strong response for long AGNRs ($N = 150$ and $N = 400$)

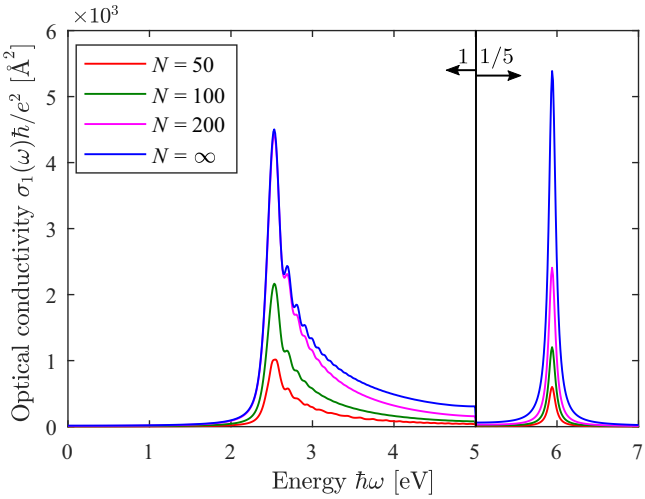


FIG. 7. Real part of linear optical conductivity for finite and infinite AGNR-3 under the effect of the longitudinal electrostatic field $F^x_{\rm dc} = 0.003$ V/Å. Note that above 5 eV, the spectra are down-scaled.

below the $2\omega$ resonance which belongs to the transition with the energy of the band gap. Furthermore, good agreement between results for finite and infinite systems is observed as the length is increased.

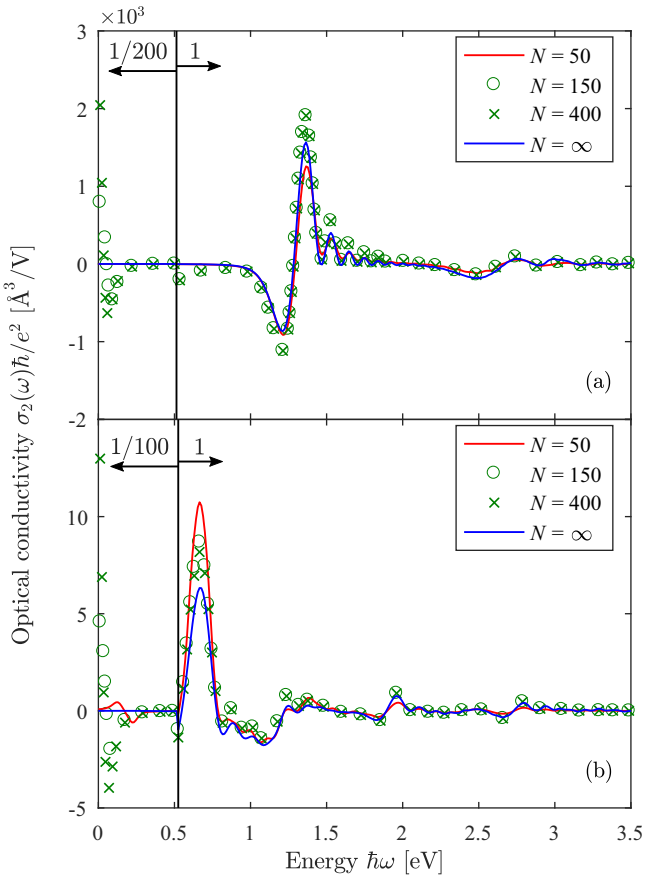


FIG. 8. Real part of second-order nonlinear optical conductivity for finite and infinite (a) AGNR-3 and (b) AGNR-9 under the effect of the longitudinal electrostatic field $F^x_{\rm dc} = 0.01$ V/Å. Note that the low-energy parts of the spectra have been down-scaled.

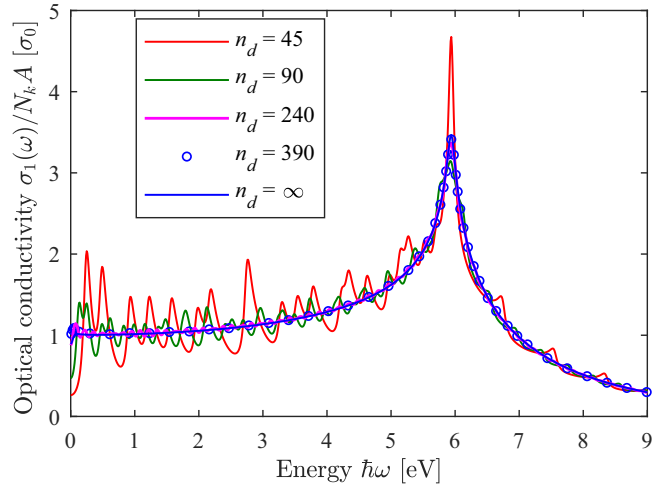


FIG. 9. Real part of linear optical conductivity for AGNR-45, AGNR-90, AGNR-240, AGNR-390, and two-dimensional graphene $n_d = \infty$.

We note that the linear and nonlinear response functions above represent the areal response of a single nanoribbon. If a macroscopic sample containing a certain density of noninteracting GNRs is considered, the total optical response can be found by accounting for the area covered by GNRs. Hence, if GNRs occupy a certain area $A$ of a large sample with area $A_{\rm tot}$, the effective response of the whole sample can be approximated by the average GNR response multiplied by $A/A_{\rm tot}$.

### B. Wide AGNRs and two-dimensional graphene

We now turn to wide AGNRs in order to study the limit as pristine graphene is approached. We obtain the linear conductivity without the effect of dc fields for wide AGNRs with various widths, i.e., AGNR-45, AGNR-90, AGNR-240, and AGNR-390 and compare them with two-dimensional graphene in Fig. 9. The results are obtained using Eq. (3) in the units of the graphene dc conductivity $\sigma_0 = e^2/4\hbar$, considering one- and two-dimensional $k$ space for AGNRs and graphene, respectively. Also, $A$ is the area of the unit cells in Fig. 1, i.e., the red area for graphene and the sum of all hexagons for AGNRs. The graphene result without field is obtained for $k$ points restricted to the irreducible Brillouin zone in Fig. 1, symmetrizing over $x$ and $y$ directions. When a field is present in graphene, $k$ summation is performed over $N_k$ points inside a rectangular Brillouin zone equivalent to the hexagonal one in Fig. 1. We add a band gap of 0.02 eV (by applying opposite on-site energies to the two sublattices) to graphene to avoid the divergence in the obtained conductivity at 0 eV. The intense peak at 5.94 eV originates from transitions at the point Γ in the Brillouin zone. The result for two-dimensional graphene agrees with previous theoretical results [53]. The figure shows that the optical response of nanoribbons approaches that of graphene for wider AGNRs.

Applying the electrostatic field $F^x_{\rm dc} = 0.01$ V/Å causes modifications in the optical response. Figure 10 shows the comparison of the linear optical conductivity for four chosen wide AGNRs and graphene under the dc field. Similarly to the zero-field result, as expected, the AGNR response con-

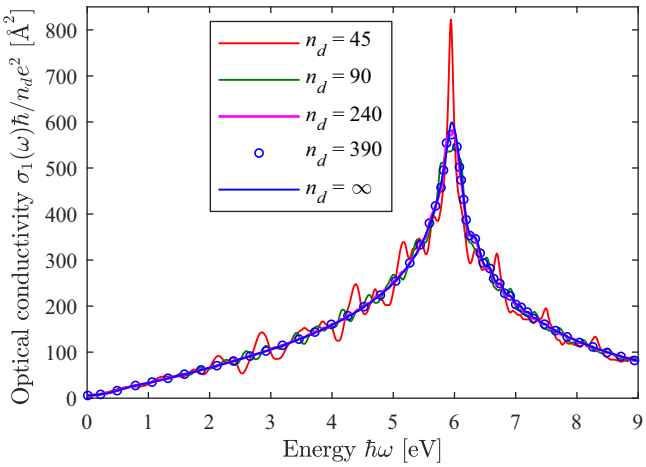


FIG. 10. Real part of linear optical conductivity for AGNR-45, AGNR-90, AGNR-240, AGNR-390, and two-dimensional graphene $n_d = \infty$ under the effect of $F^x_{\rm dc} = 0.01\,{\rm V/Å}$.

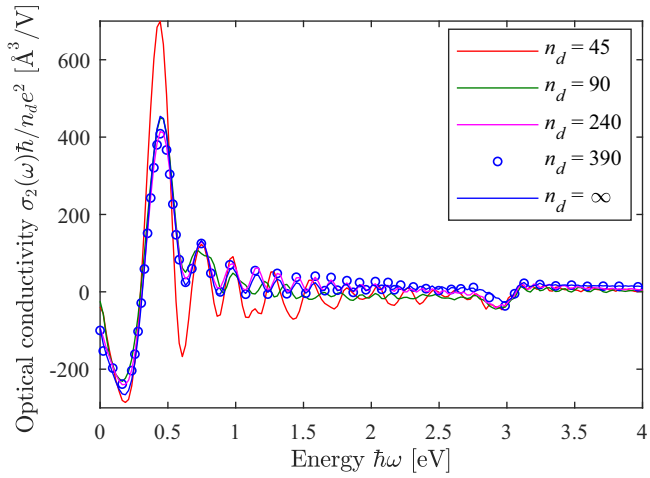


FIG. 11. Real part of second-order nonlinear optical conductivity for AGNR-45, AGNR-90, AGNR-240, AGNR-390, and two-dimensional graphene $n_d = \infty$ under the effect of $F^x_{\rm dc} = 0.01\,{\rm V/Å}$.

verges to that of graphene with increasing AGNR width. FK oscillation peaks are prominent above 5.94 eV. As expected, these oscillations are the result of transitions between WS valence and conduction states calculated in Ref. [44]. Unlike narrow AGNRs, in which oscillation peaks are visible above every absorption peak as a result of sufficient space between peaks, in graphene and wide AGNRs like AGNR-240 and AGNR-390, oscillation peaks are hidden for energies smaller than the absorption peak at the point Γ because the continuous absorption in this region smears out such oscillations. As AGNRs get narrower like AGNR-90 and AGNR-45, the results deviate more clearly from the bulk graphene result and oscillations without definite period are seen. The mixture of responses from transitions between each valence and conduction band pair and their subsequent FK oscillations result in these nondefinite oscillations.

Similar to narrow AGNRs, applying longitudinal dc fields breaks the inversion symmetry and causes a prominent second-order nonlinear response in graphene and wide AGNRs. Figure 11 shows a comparison of the second-order nonlinear optical conductivity between four selected wide AGNRs and graphene under a field of $F^x_{\rm dc} = 0.01\,{\rm V/Å}$. Similarly to the linear result, increasing the width of AGNRs results in convergence of the EFISH response to the graphene spectrum. The effect of dc fields on the nonlinear response is even more prominent than for the linear one. Considerable response below 0.5 eV followed by FK-like oscillatory peaks are observed. This shows that the dc field causes considerable one- and two-photon absorption at lower energies and related strong oscillations resulting from Eqs. (15) and (16). This energy region corresponds to transitions between the K and M points in the graphene Brillouin zone. As the photon energy increases, the oscillations weaken and one- and two-photon contributions from energies in the interval between K and Γ points change the oscillation period. Another distinct response around 3 eV is due to two-photon resonances at the Γ point followed by weaker FK-like oscillations. Similarly to the linear optical response under a longitudinal dc field, the second-order nonlinear response of the narrower AGNR-90 and AGNR-45 show nondefinite oscillation periods, in contrast to the wider AGNR-240 and AGNR-390.

## IV. SUMMARY

In summary, we have calculated the linear and nonlinear optical conductivity for narrow and wide semiconducting graphene nanoribbons and two-dimensional graphene with and without the presence of strong in-plane electrostatic fields. In narrow AGNRs, transversal fields primarily lift degeneracies in the band structure and result in associated modulations of the optical response. These modulations get stronger with increasing width of the AGNRs. Transversal fields do not break the longitudinal inversion symmetry of AGNR-3$n_d$, so there are no second-order nonlinear optical responses for this type of AGNRs.

Applying longitudinal electrostatic fields, which are along the periodic direction of the system, results in highly nonperturbative FK effects in AGNRs where we have expanded our novel density matrix method using Green's functions to multiband semiconductors. Longitudinal fields also break the centrosymmetry of AGNR-3$n_d$ and result in considerable EFISH. Moreover, both finite and infinite length AGNRs are considered in all calculations to show that the dipole moment formalism converges to the momentum method in the limit of large finite systems. In strong longitudinal fields, only finite systems of limited lengths can be considered if charge transfer between the sample ends is assumed absent. Despite this restriction, a $k$-space formalism treating infinite systems under any longitudinal dc field leads to good agreement with FK effects in large finite systems with greatly reduced computational effort. For wide AGNRs, applied longitudinal dc fields result in FK effects and considerable EFISH. By modifying the one-dimensional AGNR equations to obtain the optical response of two-dimensional graphene, linear and nonlinear optical response functions of wide AGNRs and graphene are compared and show that the AGNR responses converge to those of graphene in the limit of sufficiently wide AGNRs.

**ACKNOWLEDGMENTS**

The authors acknowledge helpful discussions with Alireza Taghizadeh, Fábio Hipólito, and Jonas Have. This work was supported by the QUSCOPE center sponsored by the Villum Foundation.

[1] L. Wang, I. Meric, P. Y. Huang, Q. Gao, Y. Gao, H. Tran, T. Taniguchi, K. Watanabe, L. M. Campos, D. A. Muller, J. Guo, P. Kim, J. Hone, K. L. Shepard, and C. R. Dean, Science **342**, 614 (2013).
[2] M. Y. Han, B. Özyilmaz, Y. Zhang, and P. Kim, Phys. Rev. Lett. **98**, 206805 (2007).
[3] B. Obradovic, R. Kotlyar, F. Heinz, P. Matagne, T. Rakshit, M. D. Giles, M. A. Stettler, and D. E. Nikonov, Appl. Phys. Lett. **88**, 142102 (2006).
[4] G. Liang, N. Neophytou, D. E. Nikonov, and M. S. Lundstrom, IEEE Trans. Electron Devices **54**, 677 (2007).
[5] Q. Yan, B. Huang, J. Yu, F. Zheng, J. Zang, J. Wu, B.-L. Gu, F. Liu, and W. Duan, Nano Lett. **7**, 1469 (2007).
[6] X. Wang, Y. Ouyang, X. Li, H. Wang, J. Guo, and H. Dai, Phys. Rev. Lett. **100**, 206803 (2008).
[7] L. Jiao, L. Zhang, X. Wang, G. Diankov, and H. Dai, Nature (London) **458**, 877 (2009).
[8] F. Bonaccorso, Z. Sun, T. Hasan, and A. C. Ferrari, Nat. Photon. **4**, 611 (2010).
[9] S. Osella, A. Narita, M. G. Schwab, Y. Hernandez, X. Feng, K. Müllen, and D. Beljonne, ACS Nano **6**, 5539 (2012).
[10] M. Mehdi Pour, A. Lashkov, A. Radocea, X. Liu, T. Sun, A. Lipatov, R. A. Korlacki, M. Shekhirev, N. R. Aluru, J. W. Lyding, V. Sysoev, and A. Sinitskii, Nat. Comm. **8**, 820 (2017).
[11] D. Kosynkin, A. Higginbotham, A. Sinitskii, J. Lomeda, A. Dimiev, B. Price, and J. Tour, Nature (London) **458**, 872 (2009).
[12] J. Cai, P. Ruffieux, R. Jaafar, M. Bieri, T. Braun, S. Blankenburg, M. Muoth, A. P. Seitsonen, M. Saleh, X. Feng, K. Müllen, and R. Fasel, Nature (London) **466**, 470 (2010).
[13] V. Abramova, A. S. Slesarev, and J. M. Tour, ACS Nano **7**, 6894 (2013).
[14] X. Li, X. Wang, L. Zhang, S. Lee, and H. Dai, Science **319**, 1229 (2008).
[15] A. Narita, X. Feng, Y. Hernandez, S. A. Jensen, M. Bonn, H. Yang, I. A. Verzhbitskiy, C. Casiraghi, M. R. Hansen, A. H. R. Koch, G. Fytas, O. Ivasenko, B. Li, K. S. Mali, T. Balandina, S. Mahesh, S. De Feyter, and K. Müllen, Nat. Chem. **6**, 126 (2013).
[16] T. H. Vo, M. Shekhirev, D. A. Kunkel, M. D. Morton, E. Berglund, L. Kong, P. M. Wilson, P. A. Dowben, A. Enders, and A. Sinitskii, Nat. Comm. **5**, 3189 (2014).
[17] V. Ryzhii, V. Mitin, M. Ryzhii, N. Ryabova, and T. Otsuji, Appl. Phys. Express **1**, 063002 (2008).
[18] W. Franz, Z. Naturforsch. A **13**, 484 (1958).
[19] L. V. Keldysh, Sov. Phys. JETP **34**, 788 (1958).
[20] Y.-W. Son, M. L. Cohen, and S. G. Louie, Phys. Rev. Lett. **97**, 216803 (2006).
[21] H. Hsu and L. E. Reichl, Phys. Rev. B **76**, 045418 (2007).
[22] W. Liao, G. Zhou, and F. Xi, J. Appl. Phys. **104**, 126105 (2008).
[23] J. Jiang, W. Lu, and J. Bernholc, Phys. Rev. Lett. **101**, 246803 (2008).
[24] K.-i. Sasaki, K. Kato, Y. Tokura, K. Oguri, and T. Sogawa, Phys. Rev. B **84**, 085458 (2011).
[25] M. Wang, Y. C. Wang, H. X. Zhao, and S. X. Song, RSC Adv. **5**, 68722 (2015).
[26] X. Zhu and M. Wang, RSC Adv. **6**, 11786 (2016).
[27] H. Raza and E. C. Kan, Phys. Rev. B **77**, 245434 (2008).
[28] W. Apel, G. Pal, and L. Schweitzer, Phys. Rev. B **83**, 125431 (2011).
[29] K. Gundra and A. Shukla, Phys. Rev. B **83**, 075413 (2011).
[30] S. Bala Kumar, T. Fujita, and G. Liang, J. Appl. Phys. **109**, 073704 (2011).
[31] H. C. Chung, C. P. Chang, C. Y. Lin, and M. F. Lin, Phys. Chem. Chem. Phys. **18**, 7573 (2016).
[32] F. Afshari and M. Ghaffarian, Physica. E: Low dimens. Syst. Nanostruct. **89**, 86 (2017).
[33] Y. C. Huang, C. P. Chang, and M. F. Lin, J. Appl. Phys. **104**, 103714 (2008).
[34] S. Bala Kumar and J. Guo, Appl. Phys. Lett. **98**, 263105 (2011).
[35] S. Bala Kumar and J. Guo, J. Appl. Phys. **110**, 044309 (2011).
[36] F. L. Shyu, Physica B: Condens. Matter **452**, 7 (2014).
[37] V. Perebeinos and P. Avouris, Nano Lett. **7**, 609 (2007).
[38] R. Alaei and M. H. Sheikhi, Fuller. Nanotub. Car. N. **21**, 183 (2013).
[39] C. H. Lee, R. K. Chang, and N. Bloembergen, Phys. Rev. Lett. **18**, 167 (1967).
[40] M. Nakano, K. Yamaguchi, Y. Matsuzaki, K. Tanaka, and T. Yamabe, Chem. Phys. Lett. **233**, 411 (1995).
[41] V. Jašinskas, M. Gedvilas, G. Račiukaitis, and V. Gulbinas, Opt. Lett. **41**, 2759 (2016).
[42] Q. Bao and K. P. Loh, ACS Nano **6**, 3677 (2012).
[43] Y. Zhou and M. W. Wu, Phys. Rev. B **83**, 245436 (2011).
[44] H. K. Kelardeh, V. Apalkov, and M. I. Stockman, Phys. Rev. B **90**, 085313 (2014).
[45] F. Bonabi and T. G. Pedersen, J. Phys.: Conden. Matter **29**, 165702 (2017).
[46] C. Aversa and J. E. Sipe, Phys. Rev. B **52**, 14636 (1995).
[47] T. G. Pedersen, Phys. Rev. B **92**, 235432 (2015).
[48] S. Reich, J. Maultzsch, C. Thomsen, and P. Ordejón, Phys. Rev. B **66**, 035412 (2002).
[49] A. Taghizadeh, F. Hipolito, and T. G. Pedersen, Phys. Rev. B **96**, 195413 (2017).
[50] J. K. Wahlstrand and J. E. Sipe, Phys. Rev. B **82**, 075206 (2010).
[51] T. G. Pedersen and T. B. Lynge, Phys. Rev. B **65**, 085201 (2002).
[52] H. Garcia, Phys. Rev. B **74**, 035212 (2006).
[53] F. Hipolito, T. G. Pedersen, and V. M. Pereira, Phys. Rev. B **94**, 045434 (2016).